

Affinity Contrastive Learning for Skeleton-based Human Activity Understanding

Hongda Liu, Yunfan Liu, Min Ren, Lin Sui, Yunlong Wang, Zhenan Sun, *Senior Member, IEEE*

Abstract—In skeleton-based human activity understanding, existing methods often adopt the contrastive learning paradigm to construct a discriminative feature space. However, many of these approaches fail to exploit the structural inter-class similarities and overlook the impact of anomalous positive samples. In this study, we introduce ACLNet, an Affinity Contrastive Learning Network that explores the intricate clustering relationships among human activity classes to improve feature discrimination. Specifically, we propose an affinity metric to refine similarity measurements, thereby forming activity superclasses that provide more informative contrastive signals. A dynamic temperature schedule is also introduced to adaptively adjust the penalty strength for various superclasses. In addition, we employ a margin-based contrastive strategy to improve the separation of hard positive and negative samples within classes. Extensive experiments on NTU RGB+D 60, NTU RGB+D 120, Kinetics-Skeleton, PKU-MMD, FineGYM, and CASIA-B demonstrate the superiority of our method in skeleton-based action recognition, gait recognition, and person re-identification. The source code is available at <https://github.com/firework8/ACLNet>.

Index Terms—Human activity understanding, Skeleton, Graph convolutional networks, Contrastive learning

I. INTRODUCTION

IN recent years, skeleton-based human activity understanding has garnered significant research attention owing to its robustness under complex environmental conditions and high computational efficiency [1], [2], [3]. Despite these advances, skeleton-based representations often suffer from inherent ambiguity when discriminating between visually similar activities, due to the absence of interacting objects (e.g., *reading* vs. *writing*) and detailed body shapes (e.g., *waving* vs. *making ok sign*). This limitation becomes especially critical in biometric applications, where subtle behavioral cues are essential for activity characterization and identity inference.

Therefore, recent methods have turned to discriminative contrastive learning techniques [4], [5], [6]. These approaches

This work was supported in part by the National Natural Science Foundation of China under Grant U23B2054, Grant 62276263, Grant 62406304, and Grant 62406028, and in part by Tianjin Key Research and Development Program CAS-Cooperation Project under Grant 24YFYSHZ00290. (Corresponding author: Zhenan Sun.)

H. Liu, Y. Wang and Z. Sun are with the Institute of Automation, Chinese Academy of Sciences, Beijing 100190, China, and H. Liu is also with the School of Artificial Intelligence, University of Chinese Academy of Sciences, Beijing 100049, China (e-mail: hongda.liu@cripac.ia.ac.cn; yunlong.wang@cripac.ia.ac.cn; znsun@nlpr.ia.ac.cn).

Y. Liu is with the School of Electronic, Electrical and Communication Engineering, University of Chinese Academy of Sciences, Beijing 101408, China (e-mail: liuyunfan@ucas.ac.cn).

M. Ren is with the School of Artificial Intelligence, Beijing University of Posts and Telecommunications, Beijing 100876, China (e-mail: minren@bupt.edu.cn).

L. Sui is with the Moonshot AI, Beijing 100086, China (e-mail: suilin0432@gmail.com).

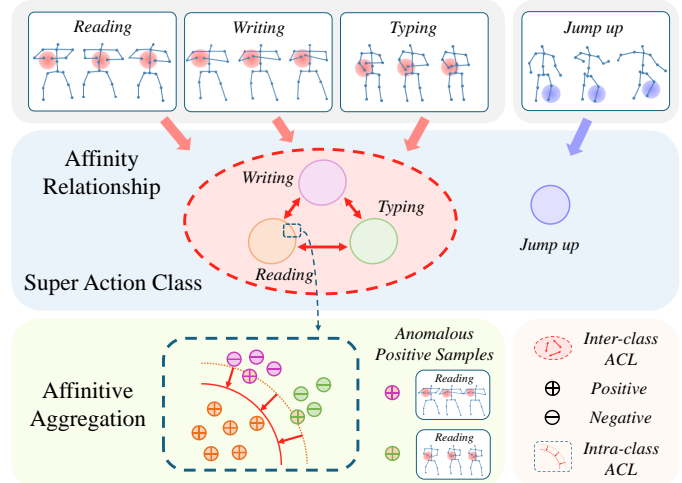


Fig. 1. Conceptual diagram for Affinity Contrastive Learning. The neglect of structural commonalities among classes and inherently anomalous positive samples within classes will degrade the performance of existing methods. Therefore, we propose Affinity Contrastive Learning to improve discriminative representations at the inter-class and intra-class levels.

either exploit global contextual cues across all skeleton sequences [4] or decouple spatial and temporal features for contrastive refinement [5]. By integrating contrastive constraints into the frameworks, they enhance the discriminability of skeleton representations. However, there are two problems with the existing contrastive learning paradigms.

First, these methods fail to exploit the potential structural similarities between activity classes. Intuitively, activities with similar motion patterns are prone to misclassification due to the commonalities in their skeleton sequences, such as common key joints or trajectories. These physical similarities are then projected into the embedding space, potentially forming clusters of similar activities across different classes. The relationships reflected in these clusters provide rich supervisory signals for contrastive learning in the embedding space. However, existing methods rely solely on global positive-negative comparisons, ignoring the exploration of the structural information. This leads to inefficient optimization, thereby limiting discriminative power in fine-grained scenarios.

Moreover, current methods neglect the inherent impact of anomalous positive samples within classes. Intra-class variability, such as differences in observation angles and movement amplitudes, inevitably introduces noise. This results in the possibility of some hard positives that are easily confused with samples from other classes. The inherent impact of these anomalous positives, coupled with the disturbance caused by negative samples from hard classes, may lead to accumulated

errors in the embedding space, ultimately degrading overall performance. This fact suggests that the learning manner for hard samples should be reformulated, however, which is not supported in the current paradigm.

To address the above issues, we introduce ACLNet, a novel affinity contrastive learning network for skeleton-based human activity understanding. First, we propose an inter-class affinity contrastive method that captures semantic commonalities among related activities. Specifically, we introduce *affinity similarity*, which measures the structural relationships between classes in the embedding space. Accordingly, these classes that consistently share similar motion patterns are grouped into higher-level superclasses, dubbed Motion Family. We then propose an inter-class affinity contrastive loss that promotes targeted refinement for semantically related classes. In addition, a dynamic family-aware temperature schedule is designed to adaptively adjust the penalty strength based on superclass size, thus enhancing representational quality.

Secondly, we propose an intra-class marginal contrastive strategy to mitigate the inherent impact of anomalous positive samples. This strategy aims to increase the marginal distance constraint between hard positives and their closest negatives, thereby encouraging affinitive aggregation for hard positives. Through controlling the minimal margin, an intra-class affinity contrastive loss is designed to achieve a better separation between positives and negatives. Fig. 1 illustrates the conceptual diagram for our affinity contrastive learning framework. Extensive experiments are conducted on six popular benchmarks, including NTU RGB+D 60, NTU RGB+D 120, Kinetics-Skeleton, PKU-MMD, and FineGYM for action recognition, as well as CASIA-B for gait recognition and person re-identification. ACLNet consistently achieves state-of-the-art performance across these benchmark datasets.

Our contributions are summarized as follows:

- We introduce ACLNet, a novel affinity contrastive learning network that enhances discriminative representations for skeleton-based human activity understanding.
- We propose an inter-class affinity contrastive method that employs the developed affinity metric to capture semantic associations between related activities, thereby enabling globally targeted refinement for hard classes.
- We present an intra-class marginal contrastive strategy to increase the minimal margin between hard positives and negatives, achieving better separation for hard samples.
- Extensive experiments demonstrate that ACLNet improves upon the current contrastive paradigm by a significant margin, proving to be superior to state-of-the-art methods on six widely used benchmarks.

II. RELATED WORK

A. Skeleton-Based Action Recognition

Early pioneering methods for skeleton-based action recognition primarily focus on recurrent neural networks (RNNs) and convolutional neural networks (CNNs) to predict class labels [1], [7], but they overlook the inherent correlations between joints. Driven by the structural characteristics of skeleton data, Graph Convolutional Networks (GCNs) have

emerged as a leading solution for skeleton-based action recognition [8], [9], [10], [11]. The first notable attempt to introduce the predefined spatial-temporal graph for modeling skeleton data is ST-GCN [12]. Although it establishes a strong baseline, the predefined graph topology poses challenges when modeling relationships between joints that lack direct connections, thereby limiting expressive capacity.

Various follow-up studies have explored more flexible modeling of joint relations, including adaptive graphs [13], [14], [15], [16], multi-scale graphs [17], [18], and channel-wise graphs [19], [20], [21], [22]. For instance, 2s-AGCN [13] proposes an adaptive graph convolutional network that learns the topology in an end-to-end manner. Subsequently, InfoGCN [20] leverages an information-theoretic objective and multiple modalities to better represent latent information. Recently, BlockGCN [23] introduces novel topological encoding schemes, which include static and dynamic encoding to identify and restore the overlooked topologies.

Nevertheless, capturing discriminative semantic features for similar classes remains a challenge for existing methods. To address this problem, we propose the affinity contrastive learning network, which imposes additional affinity constraints on hard classes and samples, enabling the model to learn more distinctive skeleton representations.

B. Skeleton-Based Behavioral Identification

Skeleton-based behavioral identification has emerged as a key subfield in biometrics, with efforts centered on gait recognition and person re-identification. Unlike generic action recognition, this task requires capturing individualized motion patterns that are unique and consistent across instances. In gait recognition, early skeleton-based approaches like PoseGait [24] use 3D keypoints to achieve view invariance. Following that, GaitGraph [25] and GaitGraph2 [26] adopt multi-branch graph frameworks to model body relationships. Recent methods such as MSGG [27], Gait-D [28], and CycleGait [29] leverage GCN-based architectures to achieve considerable performance gains. In parallel, skeleton-based person re-identification aims to match and retrieve individuals using skeletal representations. Early works manually design skeleton descriptors based on anthropometric and gait attributes [30]. Rao et al. [31] utilize an LSTM-based encoder with attention mechanisms (AGE) to learn skeletal features. Its extension SGELA [32] integrates skeletal pretext tasks and inter-sequence contrastive learning to enhance representations. Recently, TranSG [2] proposes a Transformer-based skeleton graph contrastive learning framework to capture complex skeletal relations. Compared with these methods, we introduce the affinity contrastive learning to highlight subtle differences between classes, achieving effective biometric identification. The proposed affinity modeling paradigm opens new avenues for fine-grained activity understanding, with potential applications in various behavioral biometrics tasks.

C. Contrastive Learning

Contrastive learning is a classical self-supervised representation method that has been shown to improve both performance and robustness of downstream tasks in diverse

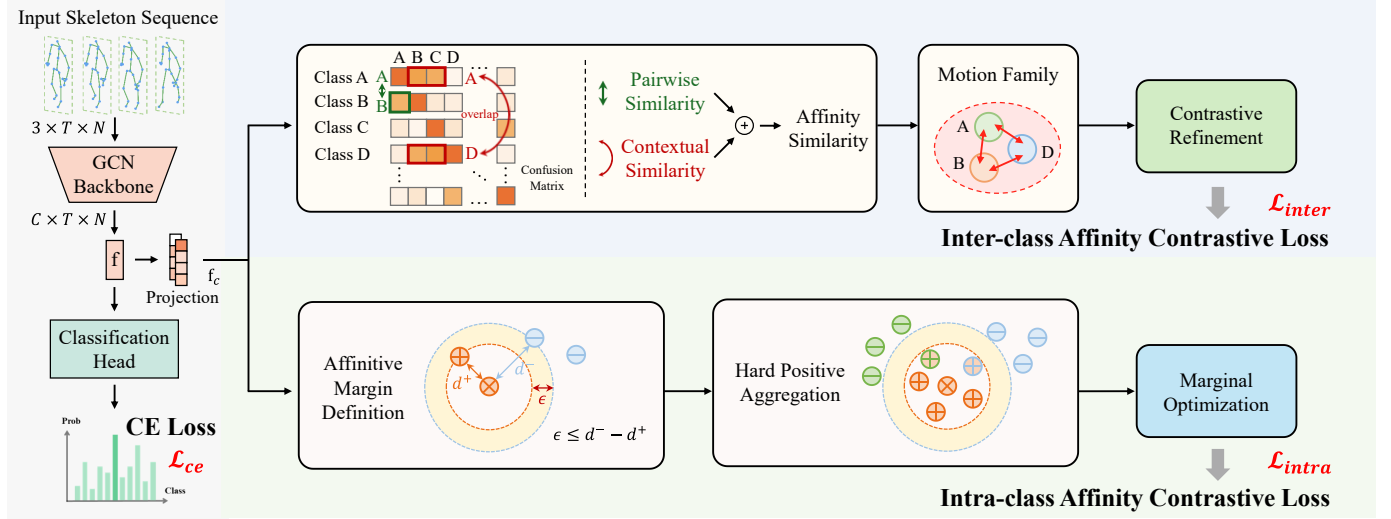


Fig. 2. The framework of the proposed ACLNet. The input skeleton sequence is fed into the GCN backbone to extract skeleton feature f , which is embedded into a vector by projection for affinity contrastive learning. Specifically, we introduce affinity similarity to measure the semantic associations between related activities while considering their pairwise and contextual similarities. The Motion Family is then constructed to enable targeted refinement for hard classes. Additionally, we define the affine margin to provide accurate control of the minimal distance between the positive sample and the closest negative sample. By increasing the margin, the optimization strategy helps to improve the separation between hard positives and negatives. Finally, the two affinity contrastive losses contribute to the construction of a discriminative feature space, effectively improving the accuracy of the model.

fields [33], [34], [35], [36]. Methods such as MoCo [33] and SimCLR [34] propose ingenious paradigms to focus on semantic representations through this contrastive learning manner. Another line of work [37], [38] focuses on metric learning, consistently bootstrapping the representation by discovering the hard positive and negative samples. Inspired by these contrastive paradigms, our work leverages the developed affinity metric and the affine margin constraint to encourage the model to learn discriminative information. In the field of skeleton-based human activity understanding, there are two research perspectives on the application of contrastive learning. In self-supervised [39], [40] and unsupervised settings [41], prior approaches utilize skeleton transformations to construct diverse positive and negative pairs, aiming to maintain consistency within the embedding space. In parallel, contrastive learning has also demonstrated considerable potential in fully supervised scenarios [4], [5], [42], [43]. Regarding the distinction of similar actions, the methodology of current works can be summarized as finding differences in actions from a specific perspective. For instance, Huang et al. [4] explicitly explore the global context information across all sequences, and Zhou et al. [5] propose spatio-temporal feature refinement to improve discriminative representations.

In contrast, our objective is to inform the recognition model which actions are semantically confusing, thereby prompting the model to focus on distinguishing them and spontaneously finding differences. The affinity information contains rich supervisory signals that can provide significant disambiguation clues. Consequently, this enables the model to effectively capture the distinctive semantics between activities.

III. METHOD

In this section, we begin by briefly introducing the preliminary concepts of skeleton-based human activity understanding

using GCNs. We then provide a detailed description of the proposed affinity contrastive learning framework. An overview of the proposed ACLNet is depicted in Fig. 2.

A. Preliminaries

The input for skeleton-based approaches is a sequence of skeletons spanning T frames, where each skeleton consists of N body joints. The human skeleton is typically represented as a graph $\mathcal{G} = (\mathcal{V}, \mathcal{E})$, where $\mathcal{V} = \{v_1, v_2, \dots, v_N\}$ is the set of body joints, \mathcal{E} represents the connectivity among these joints. In practice, \mathcal{E} is implemented as the adjacency matrix $\mathbf{A} \in \mathbb{R}^{N \times N}$, where each element a_{ij} reflects the strength of the correlation between joints v_i and v_j . The framework of GCN models can be perceived as a backbone network consisting of L stacked graph convolutional layers, followed by a classification head. The extracted semantic feature of joint motions can be denoted as $\mathbf{X} \in \mathbb{R}^{C \times T \times N}$, where C is the dimension of motion features.

Mathematically, the translation function of the l -th layer within the backbone network can be written as,

$$\mathbf{X}^{(l)} = \sigma(\mathbf{A}^{(l)} \mathbf{X}^{(l-1)} \Theta^{(l)}) \quad (1)$$

where $\mathbf{A} \in \mathbb{R}^{N \times N}$ is the adjacency matrix representing the correlations between N joints, $\Theta^{(l)} \in \mathbb{R}^{C^{(l-1)} \times C^{(l)}}$ denotes the learnable weight of the convolutional operation, and σ indicates the ReLU activation function. After obtaining the final hidden representation $\mathbf{X}^{(L)}$, a classification network is employed to determine the prediction label $\hat{\mathbf{y}} \in \mathbb{R}^c$. Here c denotes the total number of classes. The cross-entropy loss \mathcal{L}_{ce} is then applied to supervise the predicted class

$$\mathcal{L}_{ce} = - \sum_i^c \mathbf{y}_i \log \hat{\mathbf{y}}_i \quad (2)$$

where \mathbf{y}_i is the one-hot ground-truth label. Additionally, a projection layer is employed to embed the last hidden representation into the vector \mathbf{f}_c within the contrastive feature space, which is utilized in the computation of objective functions for the proposed affinity contrastive learning network.

B. Inter-class Affinity Contrastive Learning

To tackle the challenge of differentiating between activities that are prone to misclassification, we investigate the intricate inter-class relationships and introduce the concept of Motion Family. Specifically, Motion Family is the superclass formed by clustering based on the proposed *affinity similarity*, which represents the set of associated activities with structural commonalities. In the following subsections, we provide a detailed explanation of *affinity similarity* and then introduce the inter-class affinity contrastive loss.

1) *Affinity Similarity Definition*: The quality of the motion semantic associations is vital since they determine the clustering of the Motion Family. However, computing reliable semantic associations is non-trivial, especially at the early stages of the training process. To overcome this issue, we propose *affinity similarity* to estimate high-quality semantic associations between related activities.

Our key idea is to leverage not only the direct pairwise relations between the two activity classes, but also the indirect semantic commonalities via their overlap. Intuitively, if two activities share many similar classes, they should be considered to have a hidden commonality and thus be within the same superclass space. During training, recognition models can implicitly create a similarity graph between activities, and our method introduces affinity constraints on top of this graph, resulting in self-taught clustering relationships. Such implicit inter-class affinity helps to capture structural commonalities between classes and provides rich supervisory signals for further contrastive learning efficiently and concisely.

In practice, we begin by gathering misclassified samples to construct the initial confusion matrix between activity classes, which discovers the direct pairwise associations. We then capture indirect hidden commonalities by considering their overlaps in the confusion matrix. The proposed *affinity similarity* is defined as the combination of direct pairwise similarity and indirect contextual similarity. Accordingly, we split the calculation into two sequential steps.

2) *Affinity Similarity Calculation*: The first step involves calculating pairwise associations between classes by identifying confusing classes. A global statistics matrix H , initialized to zero, represents the pairwise relations between activities. Here $H_{i,j}$ indicates the number of samples belonging to class i that are misclassified as class j . Given all the inputs, this matrix helps to establish the global pairwise associations.

To reduce the impact of predictive randomness, we focus on the top K most similar classes, which are highly correlated, as pairwise candidates. The pairwise association set for class i is further defined as:

$$\mathcal{N}_K(i) = \{j | j \in \text{Top}_K(H_{i,\cdot}), j \neq i\} \quad (3)$$

where $H_{i,\cdot}$ indicates the statistics of class i with all other classes, and $\mathcal{N}_K(i)$ represents K classes with higher values

in the statistics $\text{Top}_K(H_{i,\cdot})$. Statistically, K is set to 10. Then we establish the binary matrix $\mathbb{I}_{\mathcal{N}_K}(i, j)$ indicating the pairwise similarity between class i and class j , which could be expressed as:

$$\mathbb{I}_{\mathcal{N}_K}(i, j) = \begin{cases} 1, & \text{if } j \in \mathcal{N}_K(i) \\ 0, & \text{if } j \notin \mathcal{N}_K(i) \end{cases} \quad (4)$$

Since the network is not yet mature enough to grasp the semantic relations between classes at the early stages of training, the preliminary associations are often compromised. In addition, the potential structural commonalities could provide implicit supervisory information. Therefore, we propose calculating the *affinity similarity*, as detailed below.

The second step aims to explore the indirect semantic associations and capture the final affinity relationship. We refine the contextual information by counting the number of neighbor activities that the two classes have in common. If two classes share many similar activities, they are more likely to have structural commonalities.

Consisting of pairwise and contextual similarity, the *affinity similarity* between classes i and class j could be defined as:

$$w_{ij} = \frac{\mathbb{I}_{\mathcal{N}_K}(i, j)}{2} + \frac{M(i, j)}{\sum_p \mathbb{I}_{\mathcal{N}_K}(i, p)}, \quad (5)$$

where $M(i, j) = \sum_{p=1}^K \mathbb{I}_{\mathcal{N}_K}(i, p) \mathbb{I}_{\mathcal{N}_K}(j, p)$.

Here p denotes the index of pairwise activity for class i , and $M(i, j)$ means the total number of classes that i and j have in common through the AND operation. $\sum_p \mathbb{I}_{\mathcal{N}_K}(i, p)$ represents the size of $\mathbb{I}_{\mathcal{N}_K}(i, j)$, generally $\sum_p \mathbb{I}_{\mathcal{N}_K}(i, p) = K$. In practice, we accordingly halve the pairwise correlation weight and then add it to the overlap value, finally obtaining the *affinity similarity*.

3) *Motion Family Refinement*: So far, the direct and indirect correlations between classes have been effectively explored. We then construct the Motion Family $W(i)$ as follows:

$$W(i) = \{j | w_{ij} > \frac{n_a}{K}\} \quad (6)$$

where n_a denotes the overlap threshold.

Thereafter, we refine the distinctive representations across the Motion Family, which represents the set of associated activities with common properties. For these hard classes with semantic consistency, the targeted refinement is carried out to better capture the feature differences between the member classes in the Motion Family. For each member class, we define the class representation \mathbf{m}_i , and update it with Exponential Moving Average (EMA):

$$\mathbf{m}_i = \gamma \cdot \mathbf{m}_i + (1 - \gamma) \cdot \frac{1}{n_k} \sum_{k=1}^{n_k} f_k^i \quad (7)$$

where $f_k^i \in \mathbb{R}^d$ represents the k -th feature of class i within the input batch, γ is the momentum term, and n_k is the total number of samples. Ideally, newly arrived samples of class i should converge with \mathbf{m}_i and differ from the representations of other classes. Along with the process, \mathbf{m}_i gradually becomes a stable estimation of the clustering center for class i , establishing the foundation for the subsequent refinement.

Lastly, we propose the inter-class affinity contrastive loss to optimize the inter-class learning objective. Let f_μ^i denote the feature of sample μ belonging to class i . The inter-class affinity contrastive loss could be formulated as:

$$\mathcal{L}_{inter} = -\log \frac{\exp(f_\mu^i \cdot \mathbf{m}_i / \tau_w)}{\exp(f_\mu^i \cdot \mathbf{m}_i / \tau_w) + \sum_{a \in W(i)} \exp(f_\mu^i \cdot \mathbf{m}_a / \tau_w)} \quad (8)$$

where a is the member class index, the \cdot symbol denotes the inner product operation, and $\mathbf{m}_i, \mathbf{m}_a$ denote the corresponding class representations.

4) *Discussion*: The proposed Motion Family is more of a conceptual framework than a direct mechanism for physically bringing similar classes closer together. Here, the affinity relationships serve as effective supervisory signals that guide the model to identify semantically related classes and focus on their refinement. Meanwhile, to address the inherent variability within each class, we employ average aggregation and cross-batch momentum updates, which effectively mitigate the impact of intra-class diversity and ensure stable updates.

C. Family-Aware Temperature Schedule

In contrastive learning, the models are trained to ensure that embeddings of different classes are repelled while embeddings of the same class are attracted. The strength of these attractive and repelling forces between samples is controlled by the temperature parameter, which has been found to crucially impact the quality of the learned representations [44]. Motivated by this, we consider that the penalty strength associated with different sizes of the Motion Family should also be adaptive. Therefore, we employ a dynamic temperature τ_w during training. Through the dynamic schedule, the representation quality could be improved without additional cost.

In practice, we modify τ_w according to the simplistic interval incremental schedule determined by the actual superclass size N_w . The hyperparameter K is set to 10, which corresponds to the threshold for the superclass size. The dynamic temperature τ_w could be formulated as:

$$\tau_w = \begin{cases} 0.1, & \text{if } N_w \leq K \\ 0.5, & \text{if } K < N_w \leq 2K \\ 1.0, & \text{if } N_w > 2K \end{cases} \quad (9)$$

Specifically, a relatively larger τ ($\tau_w = 1.0$) could increase the margin between clusters and facilitate the cluster-wise discrimination. In contrast, when the superclass sizes become small, a smaller τ ($\tau_w = 0.1$) could be used to amplify differences in similarity for hard negative samples in the embedding space, contributing to the instance-specific refinement within the superclass. For better smooth optimization, we add the $\tau_w = 0.5$ setting. Such a schedule results in a constant ‘family-aware switching’ between an emphasis on different superclasses, thereby ensuring that the model consistently improves separation between member classes.

D. Intra-class Affinity Contrastive Learning

Building upon the inter-class constraints, we further improve the intra-class representations. In general, abundant sample

diversity inevitably introduces intrinsic noise, which will result in the presence of hard positives that themselves are easily confused with other classes. These hard positives, along with negatives from similar classes, would lead to the accumulation of errors and degrade the overall performance.

To this end, we present an intra-class margin-based learning objective that provides more accurate control of the minimal margin between the positive sample and the closest negative sample. As shown in Fig. 2, the proposed marginal strategy can be regarded as an affinitive aggregation for all positives with the class, thereby achieving a better separation between hard positives and negatives.

Let x be the anchor of the original skeleton sample, x_u^+ a positive sample, x_v^- a negative sample, and N_v the number of negative samples. Here, positive and negative samples refer to samples belonging to the same and different classes. $s(f_m, f_n)$ is defined as the cosine similarity between the samples m and n . Since $\|f_m\|_2 = \|f_n\|_2 = 1$, the L2-distance $d(f_m, f_n) = \|f_m - f_n\|_2^2$ is smaller, and cosine similarity is larger. We denote $d(f_x, f_{x+})$ as d^+ , $d(f_x, f_{x_v^-})$ as d_v^- , and correspondingly, $s(f_x, f_{x+})$ as s^+ , $s(f_x, f_{x_v^-})$ as s_v^- . Consider first the case of a single positive sample x^+ . For the intra-class divergence, the following condition needs to be satisfied:

$$d_v^- - d^+ \geq \epsilon \quad \forall v \quad (10)$$

where $\epsilon > 0$ is the margin between positive and negative samples. The condition could be further derived:

$$d^+ - d_v^- \leq -\epsilon \iff s_v^- - s^+ \leq -\epsilon \quad \forall v \quad (11)$$

Based on InfoNCE [45], the above constraint could be transformed into an optimization problem with the max operator and the smooth approximation *LogSumExp* (LSE) operator:

$$\begin{aligned} & \max(-\epsilon, \{s_v^- - s^+\}_{v=1, \dots, N_v}) \\ & \approx -\log\left(\frac{\exp(s^+)}{\exp(s^+ - \epsilon) + \sum_v \exp(s_v^-)}\right) \end{aligned} \quad (12)$$

Then we generalize the above optimization to multiple positive samples to derive the following constraints:

$$s_v^- - s_u^+ \leq -\epsilon \quad \forall u, v \quad (13)$$

$$\sum_u \max(-\epsilon, \{s_v^- - s_u^+\}_{v=1, \dots, N_v}) \quad (14)$$

Therefore, the proposed intra-class marginal contrastive loss could be formulated as:

$$\mathcal{L}_{intra} = -\sum_u \log\left(\frac{\exp(s_u^+ / \tau)}{\exp((s_u^+ - \epsilon) / \tau) + \sum_v \exp(s_v^- / \tau)}\right) \quad (15)$$

where ϵ applies to all intra-class positives, and could achieve the separation between hard positive and negative samples.

E. Overall Objective Functions

Finally, the overall loss function used to train the model could be written as:

$$\mathcal{L} = \mathcal{L}_{ce} + \lambda_1 \mathcal{L}_{inter} + \lambda_2 \mathcal{L}_{intra} \quad (16)$$

where \mathcal{L}_{ce} is the cross-entropy loss used to supervise the predicted class. For balance, λ_1 and λ_2 are the weights assigned to the inter-class affinity contrastive loss \mathcal{L}_{inter} and the intra-class marginal contrastive loss \mathcal{L}_{intra} .

IV. EXPERIMENTS

A. Datasets

NTU RGB+D 60 [46] contains 56,880 indoor captured skeleton action samples, performed by 40 different subjects and classified into 60 classes. This dataset recommends two evaluation protocols: (1) cross-subject (X-Sub): train data are performed by 20 subjects, and test data are performed by the other 20 subjects. (2) cross-view (X-View): train data from camera views 2 and 3, and test data from camera view 1.

NTU RGB+D 120 [47] contains 114,480 skeleton action samples over 120 classes. There are also two protocols: (1) cross-subject (X-sub): skeleton samples from 53 subjects are used for training, while the remaining 53 are used for testing. (2) cross-setup (X-set): training data comes from 16 even setup IDs, and testing data comes from 16 odd setup IDs.

Kinetics-Skeleton is derived from the Kinetics 400 video dataset [48], utilizing the pose estimation toolbox to extract 240,436 training and 19,796 evaluation skeleton samples across 400 classes. We use the skeleton data released by Duan et al. [49] to evaluate the model. Following the standard evaluation protocol, Top-1 and Top-5 accuracies are reported.

PKU-MMD [50] is a comprehensive dataset for human action recognition, comprising more than 20,000 samples across 51 categories. For the X-Sub setting, 57 subjects are designated for training, while 9 subjects are reserved for testing. For the X-View setting, the middle and right views are used for training, with the left view serving as the test set.

FineGYM [51] is a large-scale fine-grained action recognition dataset with 29,000 videos of 99 gymnastic action classes, which requires action recognition methods to distinguish different sub-actions within the same video. We use the skeleton data provided by Duan et al. [49]. The mean class Top-1 accuracy is reported in the evaluation protocol.

CASIA-B [52] is a multi-view human gait dataset comprising 124 subjects, each captured from 11 camera views. For each angle, every subject has 10 sequences under three walking conditions: 6 normal walking (NM), 2 with a bag (BG), and 2 with clothes (CL). In addition, we adopt the commonly-used probe and gallery settings [30] for person re-identification. The settings are Normal (N-N), Bags (B-B), Clothes (C-C). In cross-condition settings, (C-N) denotes using the Clothes probe set and Normal gallery set, and (B-N) denotes matching the Bags probe set with the Normal gallery set. The Rank-1 accuracy is used to evaluate model performance.

B. Implementation Details

We use PyTorch and 1× RTX 3090 GPU for experiments. We take the contrastive learning model FR-Head [5] as the baseline. The SGD optimizer is employed with a Nesterov momentum of 0.9 and a weight decay of 5×10^{-4} . The epoch number is 150, and we set the batch size to 64. The initial learning rate is set to 0.1 with a cosine learning rate scheduler.

TABLE I
PERFORMANCE COMPARISONS AGAINST THE STATE-OF-THE-ART METHODS ON THE NTU RGB+D 60 DATASET IN TERMS OF CLASSIFICATION ACCURACY (%).

Methods	Publication	NTU RGB+D 60	
		X-Sub	X-View
ST-GCN [12]	AAAI 2018	81.5	88.3
2s-AGCN [13]	CVPR 2019	88.5	95.1
MS-G3D [17]	CVPR 2020	91.5	96.2
CTR-GCN [19]	ICCV 2021	92.4	96.8
EfficientGCN-B4 [53]	TPAMI 2022	92.1	96.1
InfoGCN [20]	CVPR 2022	93.0	97.1
SkeletonGCL [4]	ICLR 2023	92.8	97.1
FR-Head [5]	CVPR 2023	92.8	96.8
HD-GCN [54]	ICCV 2023	93.4	97.2
DS-GCN [16]	AAAI 2024	93.1	97.5
BlockGCN [23]	CVPR 2024	93.1	97.0
VA-AR [11]	AAAI 2025	93.1	97.2
Ours		93.6	97.7

TABLE II
PERFORMANCE COMPARISONS AGAINST THE STATE-OF-THE-ART METHODS ON THE NTU RGB+D 120 DATASET IN TERMS OF CLASSIFICATION ACCURACY (%).

Methods	Publication	NTU RGB+D 120	
		X-Sub	X-Set
ST-GCN [12]	AAAI 2018	70.7	73.2
2s-AGCN [13]	CVPR 2019	82.5	84.2
MS-G3D [17]	CVPR 2020	86.9	88.4
CTR-GCN [19]	ICCV 2021	88.9	90.6
EfficientGCN-B4 [53]	TPAMI 2022	88.7	88.9
InfoGCN [20]	CVPR 2022	89.8	91.2
SkeletonGCL [4]	ICLR 2023	89.8	91.2
FR-Head [5]	CVPR 2023	89.5	90.9
HD-GCN [54]	ICCV 2023	90.1	91.6
DS-GCN [16]	AAAI 2024	89.2	91.1
BlockGCN [23]	CVPR 2024	90.3	91.5
VA-AR [11]	AAAI 2025	90.3	91.5
Ours		90.7	92.3

To avoid instability in early training, we perform affinity calculations beginning from epoch 30. The computational complexity is closely tied to the batch size and the number of classes. In addition, γ in Eq. 7 is set to 0.9, and τ in Eq. 15 is set by default to 0.1. The dimension of feature vectors \mathbf{f}_c for contrastive learning is set to 256, and the weights λ_1 and λ_2 in Eq. 16 are set to 0.1. We use the framework and data pre-processing procedures outlined by Duan et al. [49], which perform efficient spatial and temporal augmentations. We follow the gait recognition settings and data augmentations from GaitGraph [25]. For person re-identification, we follow TranSG [2] and set the sequence length to 40 frames. The random seed is fixed to ensure experiment reproducibility.

C. Comparison with State-of-the-Art Methods

We compare ACLNet with state-of-the-art methods on six benchmark datasets, including NTU RGB+D 60, NTU

TABLE III

PERFORMANCE COMPARISONS AGAINST THE STATE-OF-THE-ART METHODS ON THE KINETICS-SKELETON DATASET IN TERMS OF CLASSIFICATION ACCURACY (%).

Methods	Publication	Kinetics-Skeleton	
		Top-1	Top-5
ST-GCN [12]	AAAI 2018	30.7	52.8
2s-AGCN [13]	CVPR 2019	36.1	58.7
MS-G3D [17]	CVPR 2020	38.0	60.9
UPS [55]	CVPR 2023	40.5	63.3
STFD-Net [56]	TCSVT 2024	48.1	-
DS-GCN [16]	AAAI 2024	50.6	-
Ours		52.1	75.9

TABLE IV

PERFORMANCE COMPARISONS WITH THE STATE-OF-THE-ART METHODS ON PKU-MMD IN TERMS OF CLASSIFICATION ACCURACY (%).

Methods	Publication	PKU-MMD	
		X-Sub	X-View
STA-LSTM [1]	TIP 2018	86.9	92.6
RF-Action [57]	ICCV 2019	92.9	94.4
ActCLR [41]	CVPR 2023	90.0	91.6
DMMG [58]	TIP 2023	91.7	-
HA-GNN [59]	TMM 2024	92.2	-
AJTP [22]	TCSVT 2024	95.0	96.7
Ours		97.3	98.7

TABLE V

PERFORMANCE COMPARISONS WITH THE STATE-OF-THE-ART METHODS ON FINEGYM IN TERMS OF CLASSIFICATION ACCURACY (%).

Methods	Publication	FineGYM
LT-S3D [60]	ECCV 2018	88.9
PoseConv3D [61]	CVPR 2022	94.3
Ske2Grid [14]	ICML 2023	91.8
SkeletonMAE [62]	ICCV 2023	91.8
VA-AR [11]	AAAI 2025	92.8
Ours		96.0

RGB+D 120, Kinetics-Skeleton, PKU-MMD, FineGYM, and CASIA-B. The proposed method consistently achieves state-of-the-art performance in all scenarios.

The results on the NTU RGB+D 60 dataset are illustrated in Table I. ACLNet achieves the best classification accuracy of 93.6% under the X-Sub setting and 97.7% under the X-View setting. Furthermore, on the challenging NTU RGB+D 120 dataset, ACLNet demonstrates comparable performance, achieving accuracies of 90.7% under the X-Sub setting and 92.3% under the X-Set setting, as shown in Table II. For Kinetics-Skeleton, it is evident from Table III that the proposed method has delivered superior performance. In addition, according to the results in Table IV and Table V, the significant improvement of the proposed ACLNet on the PKU-MMD and FineGYM datasets demonstrates its powerful ability to model diverse and complex actions. As presented in Table VI, our

TABLE VI

PERFORMANCE COMPARISONS WITH THE STATE-OF-THE-ART SKELETON-BASED GAIT RECOGNITION METHODS ON CASIA-B IN TERMS OF AVERAGED RANK-1 ACCURACY (%).

Methods	CASIA-B			
	NM	BG	CL	Avg
PoseGait [24]	68.7	44.5	36.0	49.7
GaitGraph [25]	87.7	74.8	66.3	76.3
GaitGraph2 [26]	82.0	73.2	63.6	72.9
MSGG [27]	93.0	78.1	68.3	79.8
Gait-D [28]	91.6	79.0	72.0	80.9
CycleGait [29]	92.8	84.0	78.7	85.2
Ours	94.7	85.4	85.4	88.5

TABLE VII

PERFORMANCE COMPARISON WITH THE STATE-OF-THE-ART PERSON RE-IDENTIFICATION METHODS ON CASIA-B IN TERMS OF RANK-1 ACCURACY (%).

Methods	Probe-Gallery				
	N-N	B-B	C-C	C-N	B-N
ELF [63]	12.3	5.8	19.9	5.6	17.1
MLR [30]	16.3	18.9	25.4	20.3	31.8
AGE [31]	20.8	37.1	35.5	14.6	32.4
SGELA [32]	71.8	48.1	51.2	15.9	36.4
TranSG [2]	78.5	67.1	65.6	23.0	44.1
Ours	82.8	68.5	68.0	25.2	46.5

TABLE VIII

COMPARISONS OF CLASSIFICATION ACCURACY (%) WHEN APPLYING DIFFERENT COMPONENTS UNDER THE NTU-60 X-SUB SETTING WITH THE JOINT MODALITY.

Baseline	Inter-ACL	FAT	Intra-ACL	Params	X-Sub
✓				3.56M	90.3
✓	✓			3.71M	90.9 (↑ 0.6)
✓	✓	✓		3.71M	91.1 (↑ 0.8)
✓			✓	3.68M	90.8 (↑ 0.5)
✓	✓	✓	✓	3.86M	91.4 (↑ 1.1)

method achieves competitive results compared with the representative skeleton-based gait recognition methods on CASIA-B. For person re-identification, the results in Table VII verify the effectiveness of ACLNet to learn discriminative patterns, and demonstrate the potential for biometric applications.

D. Ablation Study

In this part, we conduct ablation studies to evaluate the effectiveness of the proposed method. The experiments are performed on the NTU RGB+D 60 with the joint modality under the X-Sub and X-View settings.

1) *Effectiveness of Individual Components*: We first scrutinize the contribution of each ACLNet component in Table VIII. Specifically, the introduction of $\mathcal{L}_{\text{inter}}$ (Inter-ACL) bolsters performance by 0.6%. We also provide the additional results that when incorporating the contextual similarity, the accuracy improves from 90.5% with pairwise similarity alone to 90.9%. This shows that the intricate inter-class relationships

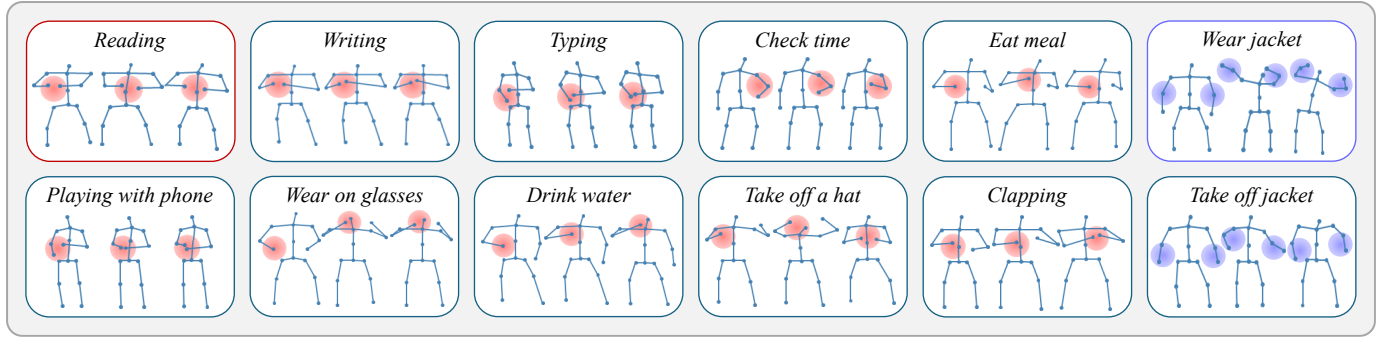


Fig. 3. Examples of Motion Family corresponding to the anchor actions ‘reading’ and ‘wear jacket’. Red and blue areas reflect the notable body parts with high learned weights, which indicate the structural commonality links (e.g., hand-related and arm-related) in the skeleton sequences.

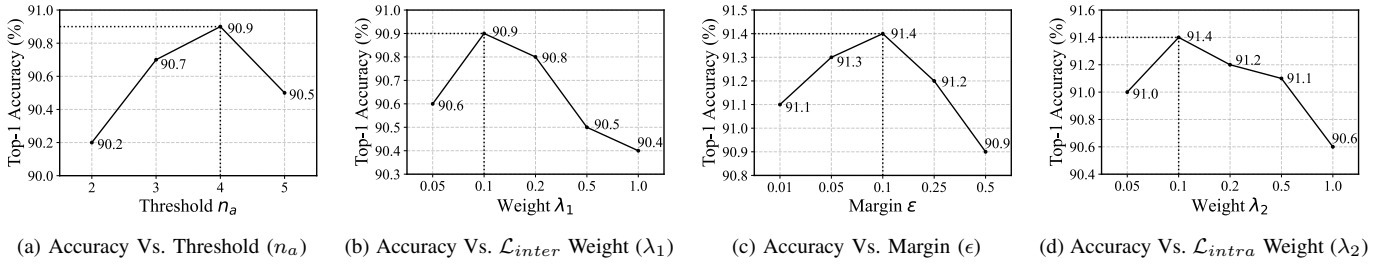


Fig. 4. Ablation study on the effect of different hyper-parameters under the NTU RGB+D 60 X-Sub setting with the joint modality.

TABLE IX
PERFORMANCE COMPARISON OF OCCLUSIONS UNDER THE NTU-60
X-SUB SETTING IN TERMS OF ACCURACY (%).

Methods	Occluded Part				
	Left Arm	Right Arm	Two Hands	Two Legs	Trunk
ST-GCN [12]	71.4	60.5	62.6	77.4	50.2
2s-AGCN [13]	72.4	55.8	82.1	74.1	71.9
RA-GCN [64]	74.5	59.4	74.2	83.2	72.3
MS-G3D [17]	31.3	23.8	17.1	78.3	61.6
CTR-GCN [19]	13.0	12.5	12.7	21.0	36.3
HD-GCN [54]	67.1	55.7	56.7	74.8	61.3
PDGCN [65]	76.0	62.0	75.4	85.0	73.0
Ours	87.1	83.3	79.6	88.5	80.5

could provide valuable supervisory signals to help distinguish classes. It is worth noting that the dynamic scheduling tailored for Inter-ACL acts primarily as hyper-parameter tuning when used alone, showing minimal impact on the baseline. Combining all the components, our full model reaches 91.4% in accuracy and surpasses the baseline by 1.1%.

2) *Implications of Motion Family:* In Fig. 3, we show the examples of Motion Family corresponding to the anchor actions ‘reading’ and ‘wear jacket’. We find that the constructed superclasses provide a good exploration of inter-class relationships between actions. The method effectively captures the hidden, valuable connections and thus makes targeted distinctions. Interestingly, it can be observed that within the Motion Family, some action classes are not intuitively related, and they appear to exhibit differences in motion patterns (e.g., reading and drinking water). This is because the construction of the Motion Family reflects the similarity matrix statis-

TABLE X
AVERAGE PERFORMANCE (%) ON DIFFERENT DIFFICULTY LEVEL CLASSES
SORTED BY ACCURACY UNDER THE NTU RGB+D 60 X-SUB SETTING.

Difficulty Level	Baseline	ACLNet	Δ
class 1-5	68.9	72.0	+3.1
class 6-15	82.2	84.8	+2.6
class 16-30	90.7	92.1	+1.4
class 31-60	96.3	96.6	+0.3

tics, highlighting shared spatial and temporal motion patterns among actions. Upon analysis, we observe that actions like reading and drinking exhibit overlapping hand trajectories, particularly when picking up objects such as books or glasses. While these actions are clearly distinct in human vision, the model may confuse them based on the skeletal data. Grouping such related actions into one family helps to refine their differentiation. This targeted refinement enhances the ability of the model to handle harder cases.

3) *Effect of Hyper-parameters:* We analyze the effect of hyper-parameters in ACLNet, and the results are shown in Fig. 4. The effect of the hyper-parameter n_a is presented in Fig. 4 (a). It can be observed that the appropriate threshold, *i.e.*, $n_a = 4$, benefits the classification performance. Then, we explore the impact of the weight λ_1 on \mathcal{L}_{inter} . As shown in Fig. 4 (b), the best performance is achieved when λ_1 is equal to 0.1. The impact of the margin ϵ is shown in Fig. 4 (c). We find that $\epsilon = 0.1$ achieves the best performance. Similarly, we examine the influences of λ_2 on \mathcal{L}_{intra} . The results in Fig. 4 (d) show that $\lambda_2 = 0.1$ gives the best performance.

4) *Robustness to Noisy Skeleton Data:* Following the research [65], we construct noisy skeleton data by simulating

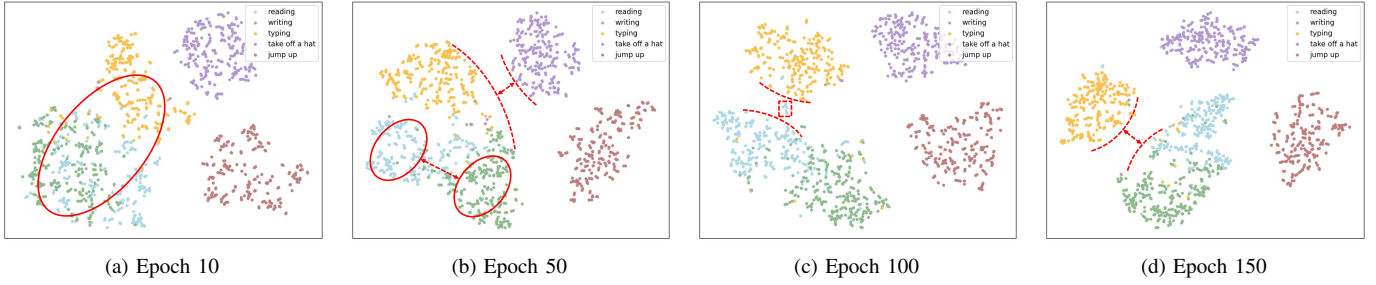
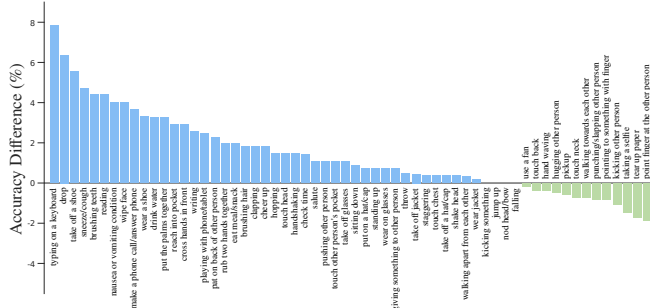


Fig. 5. The t-SNE plots of the feature embeddings for five chosen action classes throughout the training process. Colors indicate individual classes from NTU-60 X-Sub. From the early epoch (a) to later epochs (b-d), the clusters grow progressively more compact and more widely separated, revealing a steady gain in class discriminability. Best viewed with zoom in.



[6] C. Li, C. Cheng, M. Yu, Z. Liu, and D. Huang, "Joint coarse to fine-grained spatio-temporal modeling for video action recognition," *IEEE Transactions on Biometrics, Behavior, and Identity Science*, vol. 7, no. 3, pp. 444–457, 2025.

[7] B. Li, Y. Dai, X. Cheng, H. Chen, Y. Lin, and M. He, "Skeleton based action recognition using translation-scale invariant image mapping and multi-scale deep cnn," in *2017 IEEE International Conference on Multimedia & Expo Workshops (ICMEW)*. IEEE, 2017, pp. 601–604.

[8] Z. Sun, Q. Ke, H. Rahmani, M. Bennamoun, G. Wang, and J. Liu, "Human action recognition from various data modalities: A review," *IEEE Transactions on Pattern Analysis and Machine Intelligence*, vol. 45, no. 3, pp. 3200–3225, 2022.

[9] Z. Tu, J. Zhang, H. Li, Y. Chen, and J. Yuan, "Joint-bone fusion graph convolutional network for semi-supervised skeleton action recognition," *IEEE Transactions on Multimedia*, vol. 25, pp. 1819–1831, 2022.

[10] H. Liu, Y. Wang, M. Ren, J. Hu, Z. Luo, G. Hou, and Z. Sun, "Balanced representation learning for long-tailed skeleton-based action recognition," *Machine Intelligence Research*, vol. 22, no. 3, pp. 466–483, 2025.

[11] J. Wei, L. Qin, B. Yu, T. Zou, C. Yan, D. Xiao, Y. Yu, L. Yang, K. Li, and J. Liu, "Va-ar: Learning velocity-aware action representations with mixture of window attention," in *Proceedings of the AAAI Conference on Artificial Intelligence*, vol. 39, no. 8, 2025, pp. 8286–8294.

[12] S. Yan, Y. Xiong, and D. Lin, "Spatial temporal graph convolutional networks for skeleton-based action recognition," in *Proceedings of the AAAI conference on artificial intelligence*, vol. 32, 2018, pp. 1–9.

[13] L. Shi, Y. Zhang, J. Cheng, and H. Lu, "Two-stream adaptive graph convolutional networks for skeleton-based action recognition," in *Proceedings of the IEEE/CVF Conference on Computer Vision and Pattern Recognition*, 2019, pp. 12 026–12 035.

[14] D. Cai, Y. Kang, A. Yao, and Y. Chen, "Ske2grid: skeleton-to-grid representation learning for action recognition," in *International Conference on Machine Learning*. PMLR, 2023, pp. 3431–3441.

[15] J. Zhang, Z. Tu, J. Weng, J. Yuan, and B. Du, "A modular neural motion retargeting system decoupling skeleton and shape perception," *IEEE Transactions on Pattern Analysis and Machine Intelligence*, vol. 46, no. 10, pp. 6889–6904, 2024.

[16] J. Xie, Y. Meng, Y. Zhao, A. Nguyen, X. Yang, and Y. Zheng, "Dynamic semantic-based spatial graph convolution network for skeleton-based human action recognition," in *Proceedings of the AAAI Conference on Artificial Intelligence*, vol. 38, 2024, pp. 6225–6233.

[17] Z. Liu, H. Zhang, Z. Chen, Z. Wang, and W. Ouyang, "Disentangling and unifying graph convolutions for skeleton-based action recognition," in *Proceedings of the IEEE/CVF Conference on Computer Vision and Pattern Recognition*, 2020, pp. 143–152.

[18] Y. Yang, J. Zhang, J. Zhang, B. Du, and Z. Tu, "Expressive keypoints for skeleton-based action recognition via progressive skeleton evolution," *IEEE Transactions on Image Processing*, vol. 34, pp. 7585–7599, 2025.

[19] Y. Chen, Z. Zhang, C. Yuan, B. Li, Y. Deng, and W. Hu, "Channel-wise topology refinement graph convolution for skeleton-based action recognition," in *Proceedings of the IEEE/CVF International Conference on Computer Vision*, 2021, pp. 13 359–13 368.

[20] H.-g. Chi, M. H. Ha, S. Chi, S. W. Lee, Q. Huang, and K. Ramani, "Infogen: Representation learning for human skeleton-based action recognition," in *Proceedings of the IEEE/CVF Conference on Computer Vision and Pattern Recognition*, 2022, pp. 20 186–20 196.

[21] H. Duan, J. Wang, K. Chen, and D. Lin, "Dg-stgcn: Dynamic spatial-temporal modeling for skeleton-based action recognition," *arXiv preprint arXiv:2210.05895*, 2022.

[22] S. R. Gunasekara, W. Li, J. Yang, and P. O. Ogunbona, "Asynchronous joint-based temporal pooling for skeleton-based action recognition," *IEEE Transactions on Circuits and Systems for Video Technology*, vol. 35, no. 1, pp. 357–366, 2024.

[23] Y. Zhou, X. Yan, Z.-Q. Cheng, Y. Yan, Q. Dai, and X.-S. Hua, "Blockgcn: Redefine topology awareness for skeleton-based action recognition," in *Proceedings of the IEEE/CVF Conference on Computer Vision and Pattern Recognition*, 2024, pp. 2049–2058.

[24] R. Liao, S. Yu, W. An, and Y. Huang, "A model-based gait recognition method with body pose and human prior knowledge," *Pattern Recognition*, vol. 98, p. 107069, 2020.

[25] T. Teepe, A. Khan, J. Gilg, F. Herzog, S. Hörmann, and G. Rigoll, "Gaitgraph: Graph convolutional network for skeleton-based gait recognition," in *IEEE International Conference on Image Processing*. IEEE, 2021, pp. 2314–2318.

[26] T. Teepe, J. Gilg, F. Herzog, S. Hörmann, and G. Rigoll, "Towards a deeper understanding of skeleton-based gait recognition," in *Proceedings of the IEEE/CVF Conference on Computer Vision and Pattern Recognition*, 2022, pp. 1569–1577.

[27] Y. Peng, K. Ma, Y. Zhang, and Z. He, "Learning rich features for gait recognition by integrating skeletons and silhouettes," *Multimedia Tools and Applications*, vol. 83, no. 3, pp. 7273–7294, 2024.

[28] S. Gao, J. Yun, Y. Zhao, and L. Liu, "Gait-d: skeleton-based gait feature decomposition for gait recognition," *IET Computer Vision*, vol. 16, no. 2, pp. 111–125, 2022.

[29] N. Li and X. Zhao, "A strong and robust skeleton-based gait recognition method with gait periodicity priors," *IEEE Transactions on Multimedia*, vol. 25, pp. 3046–3058, 2022.

[30] Z. Liu, Z. Zhang, Q. Wu, and Y. Wang, "Enhancing person re-identification by integrating gait biometric," *Neurocomputing*, vol. 168, pp. 1144–1156, 2015.

[31] H. Rao, S. Wang, X. Hu, M. Tan, H. Da, J. Cheng, and B. Hu, "Self-supervised gait encoding with locality-aware attention for person re-identification," *arXiv preprint arXiv:2008.09435*, 2020.

[32] H. Rao, S. Wang, X. Hu, M. Tan, Y. Guo, J. Cheng, X. Liu, and B. Hu, "A self-supervised gait encoding approach with locality-awareness for 3d skeleton based person re-identification," *IEEE Transactions on Pattern Analysis and Machine Intelligence*, vol. 44, no. 10, pp. 6649–6666, 2021.

[33] K. He, H. Fan, Y. Wu, S. Xie, and R. Girshick, "Momentum contrast for unsupervised visual representation learning," in *Proceedings of the IEEE/CVF Conference on Computer Vision and Pattern Recognition*, 2020, pp. 9729–9738.

[34] T. Chen, S. Kornblith, M. Norouzi, and G. Hinton, "A simple framework for contrastive learning of visual representations," in *International Conference on Machine Learning*. PMLR, 2020, pp. 1597–1607.

[35] X. Song, S. Zhao, J. Yang, H. Yue, P. Xu, R. Hu, and H. Chai, "Spatio-temporal contrastive domain adaptation for action recognition," in *Proceedings of the IEEE/CVF Conference on Computer Vision and Pattern Recognition*, 2021, pp. 9787–9795.

[36] B. Khaertdinov, S. Asteriadis, and E. Ghaleb, "Dynamic temperature scaling in contrastive self-supervised learning for sensor-based human activity recognition," *IEEE Transactions on Biometrics, Behavior, and Identity Science*, vol. 4, no. 4, pp. 498–507, 2022.

[37] S. Kim, D. Kim, M. Cho, and S. Kwak, "Self-taught metric learning without labels," in *Proceedings of the IEEE/CVF Conference on Computer Vision and Pattern Recognition*, 2022, pp. 7431–7441.

[38] C. A. Barbato, B. Dufumier, E. Tartaglione, M. Grangetto, and P. Gori, "Unbiased supervised contrastive learning," *arXiv preprint arXiv:2211.05568*, 2022.

[39] J. Zhang, L. Lin, and J. Liu, "Prompted contrast with masked motion modeling: Towards versatile 3d action representation learning," in *Proceedings of the 31st ACM International Conference on Multimedia*, 2023, pp. 7175–7183.

[40] S. R. Gunasekara, W. Li, P. Ogunbona, and J. Yang, "Spatio-temporal joint density driven learning for skeleton-based action recognition," *IEEE Transactions on Biometrics, Behavior, and Identity Science*, vol. 7, no. 4, pp. 632–642, 2025.

[41] L. Lin, J. Zhang, and J. Liu, "Actionlet-dependent contrastive learning for unsupervised skeleton-based action recognition," in *Proceedings of the IEEE/CVF Conference on Computer Vision and Pattern Recognition*, 2023, pp. 2363–2372.

[42] H. Chang, J. Chen, Y. Li, J. Chen, and X. Zhang, "Wavelet-decoupling contrastive enhancement network for fine-grained skeleton-based action recognition," in *IEEE International Conference on Acoustics, Speech and Signal Processing*. IEEE, 2024, pp. 4060–4064.

[43] X. Bian, D. Chang, Y. Yang, Z. He, K. Liang, and Z. Ma, "Class-aware contrastive learning for fine-grained skeleton-based action recognition," in *Proceedings of the Asian Conference on Computer Vision*, 2024, pp. 3638–3654.

[44] T. Wang and P. Isola, "Understanding contrastive representation learning through alignment and uniformity on the hypersphere," in *International Conference on Machine Learning*. PMLR, 2020, pp. 9929–9939.

[45] A. v. d. Oord, Y. Li, and O. Vinyals, "Representation learning with contrastive predictive coding," *arXiv preprint arXiv:1807.03748*, 2018.

[46] A. Shahroudy, J. Liu, T.-T. Ng, and G. Wang, "Ntu rgb+ d: A large scale dataset for 3d human activity analysis," in *Proceedings of the IEEE/CVF Conference on Computer Vision and Pattern Recognition*, 2016, pp. 1010–1019.

[47] J. Liu, A. Shahroudy, M. Perez, G. Wang, L.-Y. Duan, and A. C. Kot, "Ntu rgb+ d 120: A large-scale benchmark for 3d human activity understanding," *IEEE Transactions on Pattern Analysis and Machine Intelligence*, vol. 42, no. 10, pp. 2684–2701, 2019.

- [48] W. Kay, J. Carreira, K. Simonyan, B. Zhang, C. Hillier, S. Vijayanarasimhan, F. Viola, T. Green, T. Back, P. Natsev *et al.*, “The kinetics human action video dataset,” *arXiv preprint arXiv:1705.06950*, 2017.
- [49] H. Duan, J. Wang, K. Chen, and D. Lin, “Pyskl: Towards good practices for skeleton action recognition,” in *Proceedings of the 30th ACM International Conference on Multimedia*, 2022, pp. 7351–7354.
- [50] C. Liu, Y. Hu, Y. Li, S. Song, and J. Liu, “Pku-mmd: A large scale benchmark for continuous multi-modal human action understanding,” *arXiv preprint arXiv:1703.07475*, 2017.
- [51] D. Shao, Y. Zhao, B. Dai, and D. Lin, “Finegym: A hierarchical video dataset for fine-grained action understanding,” in *Proceedings of the IEEE/CVF Conference on Computer Vision and Pattern Recognition*, 2020, pp. 2616–2625.
- [52] S. Yu, D. Tan, and T. Tan, “A framework for evaluating the effect of view angle, clothing and carrying condition on gait recognition,” in *International Conference on Pattern Recognition*, vol. 4. IEEE, 2006, pp. 441–444.
- [53] Y.-F. Song, Z. Zhang, C. Shan, and L. Wang, “Constructing stronger and faster baselines for skeleton-based action recognition,” *IEEE Transactions on Pattern Analysis and Machine Intelligence*, vol. 45, no. 2, pp. 1474–1488, 2022.
- [54] J. Lee, M. Lee, D. Lee, and S. Lee, “Hierarchically decomposed graph convolutional networks for skeleton-based action recognition,” in *Proceedings of the IEEE/CVF International Conference on Computer Vision*, 2023, pp. 10444–10453.
- [55] L. G. Foo, T. Li, H. Rahmani, Q. Ke, and J. Liu, “Unified pose sequence modeling,” in *Proceedings of the IEEE/CVF Conference on Computer Vision and Pattern Recognition*, 2023, pp. 13019–13030.
- [56] Z. Zhao, Z. Chen, J. Li, X. Wang, X. Xie, L. Huang, W. Zhang, and G. Shi, “Glimpse and zoom: Spatio-temporal focused dynamic network for skeleton-based action recognition,” *IEEE Transactions on Circuits and Systems for Video Technology*, vol. 34, no. 7, pp. 5616–5629, 2024.
- [57] T. Li, L. Fan, M. Zhao, Y. Liu, and D. Katabi, “Making the invisible visible: Action recognition through walls and occlusions,” in *Proceedings of the IEEE/CVF International Conference on Computer Vision*, 2019, pp. 872–881.
- [58] S. Guan, X. Yu, W. Huang, G. Fang, and H. Lu, “Dmmg: dual min-max games for self-supervised skeleton-based action recognition,” *IEEE Transactions on Image Processing*, vol. 33, pp. 395–407, 2023.
- [59] P. Geng, X. Lu, W. Li, and L. Lyu, “Hierarchical aggregated graph neural network for skeleton-based action recognition,” *IEEE Transactions on Multimedia*, vol. 26, pp. 11003–11017, 2024.
- [60] S. Xie, C. Sun, J. Huang, Z. Tu, and K. Murphy, “Rethinking spatiotemporal feature learning: Speed-accuracy trade-offs in video classification,” in *European Conference on Computer Vision*, 2018, pp. 305–321.
- [61] H. Duan, Y. Zhao, K. Chen, D. Lin, and B. Dai, “Revisiting skeleton-based action recognition,” in *Proceedings of the IEEE/CVF Conference on Computer Vision and Pattern Recognition*, 2022, pp. 2969–2978.
- [62] H. Yan, Y. Liu, Y. Wei, Z. Li, G. Li, and L. Lin, “Skeletonmae: graph-based masked autoencoder for skeleton sequence pre-training,” in *Proceedings of the IEEE/CVF International Conference on Computer Vision*, 2023, pp. 5606–5618.
- [63] D. Gray and H. Tao, “Viewpoint invariant pedestrian recognition with an ensemble of localized features,” in *European Conference on Computer Vision*. Springer, 2008, pp. 262–275.
- [64] Y.-F. Song, Z. Zhang, C. Shan, and L. Wang, “Richly activated graph convolutional network for robust skeleton-based action recognition,” *IEEE Transactions on Circuits and Systems for Video Technology*, vol. 31, no. 5, pp. 1915–1925, 2020.
- [65] Z. Chen, H. Wang, and J. Gui, “Occluded skeleton-based human action recognition with dual inhibition training,” in *Proceedings of the 31st ACM International Conference on Multimedia*, 2023, pp. 2625–2634.